EFFECT OF PROCESSING PARAMETERS ON THE SYNTHESIS OF LIGNIN-BASED GRAPHENE-ENCAPSULATED COPPER NANOPARTICLES

Weiqi Leng†
Post-doctoral Fellow
USDA Forest Service, Forest Products Laboratory
Madison, WI 53726
E-mail: weiqi.leng@maine.edu

H. Michael Barnes†
Thompson Distinguished Professor
E-mail: mike.barnes@msstate.edu

*Jilei Zhang**†
Professor
Department of Sustainable Bioproducts
Mississippi State University
Mississippi State, MS 39762
E-mail: jz27@msstate.edu

Zhiyong Cai†
Supervisory Materials Research Engineer, Engineered Composites Science
USDA Forest Service, Forest Products Laboratory,
Madison, WI 53726
E-mail: zcai@fs.fed.us

(Received July 2016)

Abstract. Graphene-encapsulated copper nanoparticles (GECNs) can be applied in the wood protection industry. In this study, a simple thermal treatment was applied to a mixture of kraft lignin and copper sulfate for the synthesis of GECNs. The effect of temperature, duration time, temperature rising ramp, and argon gas flow rate were investigated on the quality of the GECNs. Temperature was found to be the most important factor in the growth of graphene; high temperature was preferred to obtain less defective graphene shells. Gas flow rate, duration time, and temperature rising ramp had less effect. The optimum synthesis parameters were proposed as 1000 C, 30-min duration time, 20 C/min temperature rising ramp, and 1200-sccm argon gas flow rate. Results showed that postheat treatment was a feasible way to improve the crystallinity of graphite.

Keywords: Effect, temperature, graphene-encapsulated copper nanoparticles.

INTRODUCTION

Because of their noble properties and potential applications from composite products to the biomedical area, graphene-encapsulated metal nanoparticles (GEMNs) have been extensively studied by scientists (Host 1998). The unique core-shell structure also enables the GEMNs to be applicable in harsh environment because of the protection of the graphene shells (Wu 2003). Several methods have been used to synthesize the GEMNs including chemical vapor deposition (Wang et al 2012), flame spray synthesis (Athanassiou et al 2006), tungsten arc synthesis (Host 1998), explosion method (Wu 2003), pulsed laser deposition (Wang 2013), cation exchange (Gotoh et al 2011),

* Corresponding author
† SWST member

and thermal treatment (Mun et al 2013) among others. The phase of the raw carbon sources could be gaseous, liquid, or solid, depending on the specific method applied. The catalyst is from the transition metals group. Experimental parameters that control the synthesis process are critical to the quality of the final products. Nevertheless, they were not fully investigated. Temperature, gas flow, rising ramp, etc. all contributed to the quality of the synthesized products, including thickness, number of layers, morphology, and crystallinity of graphene (Sun et al 2012).

In this study, a simple thermal treatment was applied to a mixture of kraft lignin and copper sulfate to synthesize graphene-encapsulated copper nanoparticles (GECNs). An orthogonal experimental designed was adopted to evaluate the effect of temperature, duration time, rising ramp, and gas flow rate. X-ray diffraction spectroscopy (XRD), scanning electron microscopy (SEM), transmission electron microscopy (TEM), Raman spectroscopy, thermogravimetric analysis (TGA), and Fourier transform infrared (FTIR) spectroscopy were used for the characterization of GECNs' morphology, crystallinity, and thermal stability. The effect of each factor was discussed in detail and the optimum process combination was suggested.

MATERIALS AND METHODS

Synthesis of GECNs

Deionized water purified BioChoice Lignin (BCL-DI, 97.1% pure, ash content 0.2%, sulfur content 0.03%) was provided by Domtar Corp. (Plymouth, NC). Copper sulfate pentahydrate ($CuSO_4$ $5H_2O$, > 98%) was procured from Sigma Aldrich (St. Louis, MO). One part of $CuSO_4$ $5H_2O$ and four parts of BCL-DI (oven-dry w/w basis, the weight of Cu was used to calculate the ratio between $CuSO_4$ $5H_2O$ and BCL-DI) were dissolved into 10 parts of distilled water. The mixture was heated at 80 C and kept stirring on a hot plate stirrer for 12 h, followed by 24 h oven-drying at 103 C. After that the mixture was ground in a mortar and pestle and stored in glass vial for later use.

Two porcelain boats, each holding around 1.5 g Cu-lignin mixture, were placed into a 2 inch diameter, 32-feet-long quartz tube within the heating area. The end of tube was connected with an exhaust pipe and sealed with aluminum tape. Before heating, air in the system was excluded by flowing argon gas for 15 min at a flow rate of 1800 sccm. Temperature was raised to a specific point at a specific ramping rate, and was held for a specific time (Table 1), after which the sample was cooled down naturally, and then transferred to a desiccant. Argon gas was flowing during the whole process. The final weight of both samples was recorded and yield was calculated. Three replicates were produced in each trial. Detailed synthesis parameters are shown in Table 1, which was a $L_9(3^4)$ orthogonal array experimental design with four three-level factors considered.

The purification process was described as follows:

For each trial, 0.5 g GECNs was dissolved into 30 mL 20% HNO_3 solution in a 125-mL conical flask. The suspension was then heated up to the boiling point and kept boiling and stirring for 30 min. The suspension was filtered by a membrane (pore size: 0.45 μm) (VWR, Radnor, PA) and rinsed with 550 mL deionized water. The residue was dried in the oven at 60 C for 6 h and then 103 C for 24 h, weighed again, and stored in a glass vial for characterization.

Table 1. Experimental design for the synthesis of graphene-encapsulated copper nanoparticles.

	Factors			
Trial number	Temperature (C)	Time (min)	Ramp (C/min)	Argo flow rate (sccm)
OE-1	600	30	10	600
OE-2	600	60	15	1200
OE-3	600	90	20	1800
OE-4	800	30	15	1800
OE-5	800	60	20	600
OE-6	800	90	10	1200
OE-7	1000	30	20	1200
OE-8	1000	60	10	1800
OE-9	1000	90	15	600

OE-1 stands for Orthogonal Experiment group No. 1.

Characterization

X-ray diffraction characterization. GECNs powder was ground and analyzed with Rigaku SmartLab X-ray diffractometer (Rigaku, Woodlands, TX) using Cu Kα radiation (λ = 1.5418 Å). The scanning range was from 10 to 90 , with a scan speed of 1 /min. Gaussian function was applied to fit the curve. The crystallinity was calculated as

$$W_c = \frac{A_c}{A_c + A_a} \quad (1)$$

where W_c was the crystallinity (%), and the peaks of graphite at $2\theta = 26.2$, 42.2 , and 46.4 were categorized as the crystalline region, denoted A_c (α1), whereas the rest of the carbon peaks were categorized as the amorphous one, denominated as A_a (α1).

Microscopy. SEM characterization was completed on a JEOL JSM-6500F (JEOL, Peabody, MA). Sample was mounted on carbon tape, and coated with platinum to improve its electric conductivity. TEM characterization was completed on the JOEL JEM-2100F (JEOL). First, the sample was dissolved into acetone and sonicated for 15 min. One drop of the suspension was then dripped onto a 300 mesh copper grid with lacey carbon film (Agar Scientific, Stansted, UK), and air-dried overnight before the characterization.

Spectroscopic analysis. FTIR analysis was conducted by Thermo Scientific™ Nicolet™ iS™50 FT-IR Spectrometer (Thermo Scientific, Waltham, MA). Each spectrum was obtained in 3 s and the scanning range was from 4000 to 400 cm ^{1}. Raman spectra were collected on the LabRAM Aramis Horiba Jobin Yvon Confocal Raman Microscope (Chicago, IL), with a 532-nm green laser. The scope was set at the magnification of 100 , fast mapping mode, and four excitement sources were used.

Thermal gravimetric analysis. TGA was conducted in a TGA-50H (Shimadzu, Columbia, MD) with isothermal analyses. The system was heated up to 700 C at the ramping rate of 10 C/min. The change in mass was then related to the temperature changes during calcination. N_2 gas (99.999% purity) was flown through the TGA machine at a rate of 50 sccm.

Carbonization yield calculation.

$$\text{Yield} = [(m_{ma} \quad m_b) - (m_{mb} \quad m_b) \times 64/416 \\ /[(m_{mb} \quad m_b) \times 256/416 \quad 100 \quad (2)$$

where m_{ma} represents the mass of the boat and sample after the thermal treatment; m_b represents the mass of the boat; m_{mb} represents the mass of the boat and sample before the thermal treatment; 64/416 represents the fraction of copper in the mixture; and 256/416 represents the fraction of carbon source in the mixture.

Posttherm al Treatment of the Synthesized GECNs

GECNs synthesized under trial OE-7 were used as the raw material in this experiment. The equipment used to heat the sample was the same as that in the GECNs synthesis process, except that samples were heated in air. Three temperatures were selected (200 C, 300 C, and 500 C). XRD spectra and TEM images were obtained thereafter.

RESULTS AND DISCUSSION

The Carbonization Yield

The carbonization yield was calculated based on two assumptions: 1) No reaction occurred during the mixing of lignin and copper sulfate and 2) Copper mass remained constant during the carbonization process, whereas sulfur and oxygen were excluded in the gaseous form from the system.

The carbonization yield for all groups ranged between 43% and 50%. Figure 1 shows that the yield decreased with an increase in temperature, except for group OE-5. Heat facilitates the decomposition of lignin and generates more gas. At low and medium temperature range (600 C and 800 C), time, ramp, and argon flow rate also affect the yield. Medium duration time (60 min), fast ramp (20 C/min), and low flow rate of argon gas (600 sccm) were favorable for the decomposition of lignin. Shorter time

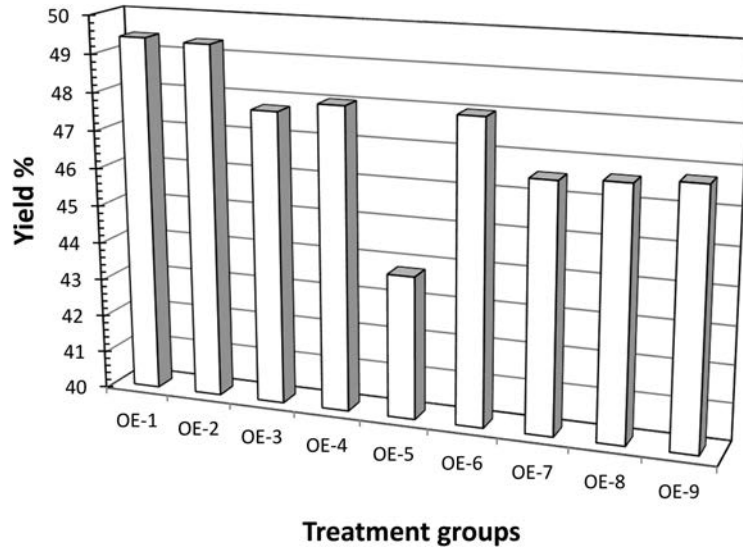

Figure 1. Carbonization yield for different treatment groups.

rendered incomplete decomposition of lignin, whereas longer time did not decompose more lignin, since the growth of graphene layers was saturated. Fast ramp raised the temperature to the target point quickly, so that less side reactions occurred during the temperature rise. Fast argon gas flow rate was not preferred, because argon gas would carry more carbonaceous gas out of the reaction region, which resulted into incomplete synthesis of GECNs. However, temperature dominated the yield when the Cu-lignin mixture was heated at 1000 C, and the yield was almost the same, irrespective of other parameters were.

X-ray Diffraction Spectra

Figure 2 shows the XRD of HNO_3-purified GECNs for all nine orthogonal treatment groups. There is a broad peak at $2\theta = 24$, which was a fitted peak for both graphite (0 0 2) at approximately $2\theta = 26.2$ (Ou et al 2008) and amorphous carbon at $2\theta = 20\text{-}27$. Figure 2 reveals that with the increase of temperature, the peak at $2\theta = 24$ became sharper, indicating higher crystallinity of the sample. The crystallinity results are shown in Table 2. Data in each cell of rows I, II, and III originate from the summation of crystallinity in respective level (I, II, or III) within each factor. For example, the data in the row II for the factor time (9.95) are the sum of crystallinity in all three level IIs within the column of factor time (row OE-2, OE-5, and OE-8), which equals to $2.44 + 2.68 + 4.83 = 9.95$. K_{I}, K_{II}, and K_{III} are the one-third of corresponding I, II, and III, respectively. The K value can be used to determine the optimal level and the optimal combination of factors. The optimal level of each factor has the highest value of K among the three values within each factor column. For instance, the highest value of 5.30% in the column of temperature indicates that level III of temperature is the optimal level among the three temperature levels, and it should be selected for the optimal combination of four factors. It is also concluded that the optimal levels for factors time, ramp rate, and argon flow rate are I, III, and II, respectively. Therefore, the optimal combination that yields the highest crystallinity is 1000 C, 30 min, 20 C/min, and 1200 sccm. The highest crystallinity obtained from this experiment is 8.73% (Table 2).

The value of R (Table 2) is defined as the difference between the maximum and minimum K value in each column. Higher R value indicates more importance of that specific factor on the crystallinity of the GECNs. Therefore, temperature has the most important impact on the

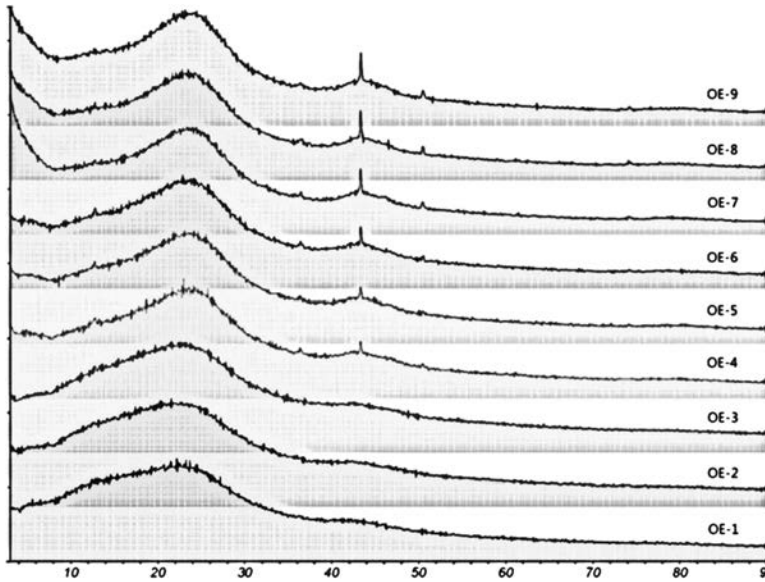

Figure 2. X-ray diffraction spectra of HNO_3-purified graphene-encapsulated copper nanoparticles (OE-1 to OE-9).

crystallinity of GECNs, followed by argon flow rate, time, and ramp rate.

Temperature was the most important factor that affected the crystallinity, with the highest *R* value (3.85). The crystallinity went higher with the increase of temperature. Graphene consists of C=C bonds. The bond energy of C–C bond is 347 kJ/mol, and that of C=C bond is 614 kJ/mol (Tarendash 2006). High temperature provided more possibility of converting C–C bond into C=C bonds, thus increasing the crystallinity of the synthesized products. The second important factor was the argon flow rate. Medium flow rate was favorable, too fast or too slow would impact the gaseous carbon deposition on the copper surface. We proposed the synthesis mechanism in another article, which stated that gaseous carbon did not help in the graphene growth process attributable to limited amount of gaseous carbon at the critical temperature. Appropriate amount of carbon atoms were required for the graphene growth fast gas flow rate resulted in few available carbon atoms; slow gas flow rate generated excessive carbon atoms deposited on the surface of copper nanoparticles, which passivated the surface, and increased the amount of amorphous carbon (Chen and Hsieh 2014).

Table 2. X-ray diffraction results.

	Factors				
Trial number	Temperature (C)	Time (min)	Ramp (C/min)	Argon flow rate (sccm)	Crystallinity (%)
OE-1	600 (I)	30 (I)	10 (I)	600 (I)	0.44
OE-2	600 (I)	60 (II)	15 (II)	1200 (II)	2.44
OE-3	600 (I)	90 (III)	20 (III)	1800 (III)	1.47
OE-4	800 (II)	30 (I)	15 (II)	1800 (III)	4.12
OE-5	800 (II)	60 (II)	20 (III)	600 (I)	2.68
OE-6	800 (II)	90 (III)	10 (I)	1200 (II)	2.5
OE-7	1000 (III)	30 (I)	20 (III)	1200 (II)	8.73
OE-8	1000 (III)	60 (II)	10 (I)	1800 (III)	4.83
OE-9	1000 (III)	90 (III)	15 (II)	600 (I)	2.33
I	4.35	13.29	7.77	5.45	T = 29.54
II	9.30	9.95	8.89	13.67	
III	15.89	6.30	12.88	10.42	
K_I	1.45	4.43	2.59	1.82	
K_{II}	3.10	3.32	2.96	4.56	
K_{III}	5.30	2.10	4.29	3.47	
R	3.85	2.33	1.70	2.74	

Duration time had less impact on the crystallinity. Results indicated that short duration time was preferred. There might be side reactions on the final products if the duration time was long, introducing more defects, as suggested by Chae et al (2009). The least important factor was the temperature ramp. Data showed that the faster the ramp temperature, the higher the crystallinity.

This result agreed with the short duration time theory: fast temperature rising ramp equals to that sample was heated up to a specific temperature quickly, so that the sample had a short exposure to heat. The optimum combination of the synthesis parameters was 1000 C, 30 min duration time, 20 C/min temperature rising ramp, and 1200-sccm gas flow rate.

The sharp peak at $2\theta = 43.3$ was assigned to Cu (111) (Huang et al 2009), indicating that the Cu^{2+} was reduced to zero valence during the thermal treatment. Copper nanoparticles heated at 600 C were washed out after the HNO_3 purification, implying that the copper nanoparticles were not flawlessly encapsulated by the graphene layers, similar to that at lower temperature range (300-500 C). The perfectness of the graphene shell was correlated to the heating temperature: the higher the temperature, the shaper the peak of Cu (111) was found, hence that the fewer defects the graphene layers had. At 1000 C, there was not much difference in the leaching of copper nanoparticles, since the intensity of the peak of Cu (111) was about the same, irrespective of the duration time, ramp, and gas flow rate were, similar results were found with the carbonization yield at 1000 C.

FTIR and Raman Spectra

Figure 3 shows the FTIR spectra of the BCL-DI lignin control and heat treated samples. In the typical BCL-DI lignin spectrum, the peak at around 3450 cm ^{1} represents the O–H stretch. The one at 2900 cm ^{1} is the C–H stretch; the one at 2260 cm ^{1} is the typical C C stretch. In the fingerprint region, the peaks at 1700 cm ^{1} and 1230 cm ^{1} are assigned to the C=O stretches. Both peaks at around 1600 cm ^{1} and 1500 cm ^{1} are characteristic for aromatic C=C ring vibration, which is the basic skeleton of lignin (Zhou et al 2011). The peaks at 1450 cm ^{1}, 1420 cm ^{1}, 1200 cm ^{1}, and 800 cm ^{1} indicate the C–H deformation, of which, the one at 1450 cm ^{1} is from methylene C–H bend, the one at 1420 cm ^{1} is assigned to vinyl C–H in plane bend, the one at 1200 cm ^{1} is the aromatic C–H in plane bend, whereas the one at 800 cm ^{1} is the aromatic C–H out of plane bend. The spectrum peaks at 1250 cm ^{1} and 1050 cm ^{1} represent the aromatic

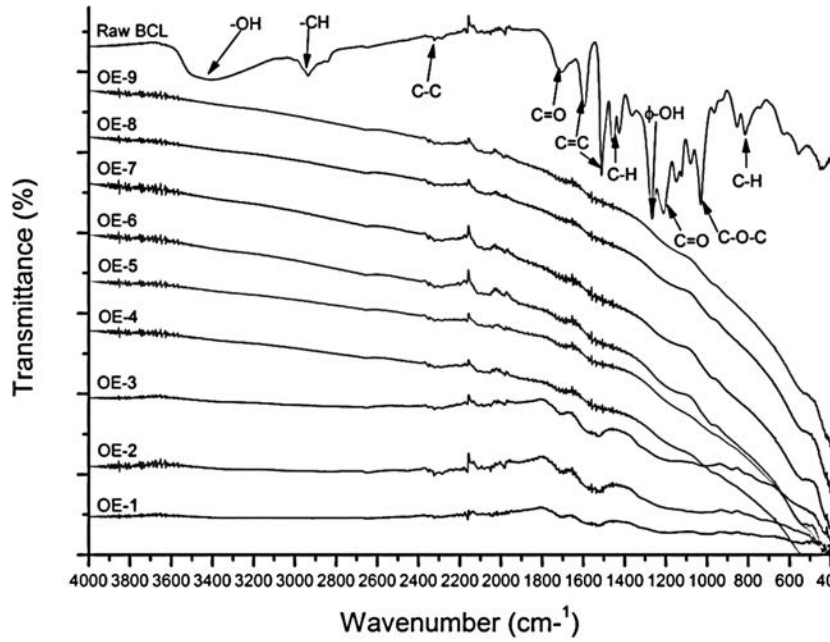

Figure 3. Fourier transform infrared spectra (Raw BCL-DI lignin and groups OE-1 to OE-9).

O–H stretch and alkyl-substituted C–O–C stretch, respectively. C–C skeletal vibration is shown at 1150 cm ^{1} (Coates 2000).

The spectrum of the sample treated at 600 C was slightly different from samples treated at higher temperature, with sharper peaks of C=O, aromatic C=C, and aromatic C–H bonds located at 1700 cm ^{1}, 1500 cm ^{1}, and 700-900 cm ^{1}, respectively. The C C peak at 2260 cm ^{1} did not change for all treatment combinations. C=O bond was the main source that would be converted into CO and CO_2 gas by annealing. However, for lignin, the converting temperature from C=O bond to gas was higher than 600 C (Yang et al 2007), which was the reason that there still was a C=O peak in the spectrum collected at 600 C. The aromatic C=C bond at around 1600 cm ^{1} was stable during mild annealing conditions. With the increase of temperature, the intensity of C=C peak continued to decrease.

The peak of O–CH_3 was close to that of C=C. However, in this spectrum, we considered there was only C=C peak, since that O–CH_3 started to convert into CH_4 at low temperatures from 280 C to 520 C (Yang et al 2007), which should be excluded from the system when reaching the higher temperature range.

Raman spectra for samples treated at groups 1, 4, and 7 are shown in Fig 4. There is a peak at around 1350 cm ^{1}, which was known as the D peak. D peak was reflected by the defective sites, which might be caused by the disordered sp^2 carbon configuration or curvature strain (Lee et al 2013). There is another peak at about 1590 cm ^{1}, knows as the G peak, which was indicated as the graphene layer. The ratio of I_D/I_G was used to evaluate the perfectness of GECNs synthesized. We can conclude from Table 3 that for all the three treatment groups, the degree of defect was reduced after HNO_3 purification. HNO_3 acted as an extracting medium to remove excessive amorphous carbon, hence the intensity of D peak reduced.

Table 3 also shows that the sample treated at 800 C has the least I_D/I_G ratio, which was not consistent with the XRD result. It was supposed that the defects of the GECNs are less at higher

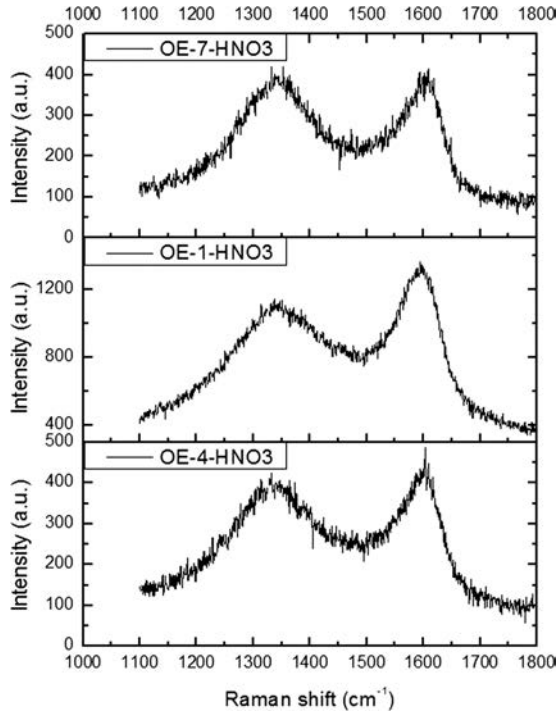

Figure 4. Raman spectra (OE-1, OE-4, and OE-7 after HNO_3 purification).

temperatures. The reason for the contradiction might originate from the size of laser beam and the sensitivity of the Raman spectrometry, which recognized more area as the defect region.

Electron Microscope Characterization

It was difficult to locate the graphene structure under TEM when the sample was heat treated at low temperature (600 C). The graphene layer was disordered, and only a few copper nanoparticles that were shelled with graphene were located. When exposed to heat for longer times, higher temperature rising ramp, and faster gas

Table 3. Ratio of I_D/I_G from Raman spectra analysis.

Sample ID	I_D (a.u)	I_G (a.u)	I_D/I_G
OE-1	1956.73	2453.60	0.88
OE-1-HNO_3	1112.62	1271.41	0.88
OE-4	429.64	433.54	0.99
OE-4-HNO_3	412.59	486.11	0.85
OE-7	546.33	516.25	1.06
OE-7-HNO_3	383.10	413.76	0.93

flow rates, it was easier to locate the graphene layers, some of which were netted with others and formed complicate structures.

With the increase of temperature (600 C → 800 C → 1000 C), more GECNs were found. Especially for the sample treated at 1000 C, large number of copper nanoparticles shelled with graphene layers were found, along with several empty graphene shells (Fig 5). The number of graphene layers was around 2-3, which was smaller than those treated with active transition metals such as iron, nickel, cobalt, etc. The difference in the number of graphene layers was attributable to fundamental growth mechanism (Zou et al 2013; Leng et al 2016). Compared with iron, copper has poor dissolving capacity of carbon; the plastic lignin film could barely be dissolved into copper atoms, while only covering the surface of copper nanoparticles and isolated from any other contact. The low dissolving capacity has limited the number of graphene layers that could be synthesized.

Figure 5 shows that the size of the copper nanoparticles and the empty graphene shells was around 10 nm, which is promising for some applications, for example, wood preservation. The size of preservative should be smaller than the size of pits to pass through and arrive to the target cell wall. Other applications that require larger particle size could be achieved by using active transition metals such as iron, nickel as catalysts.

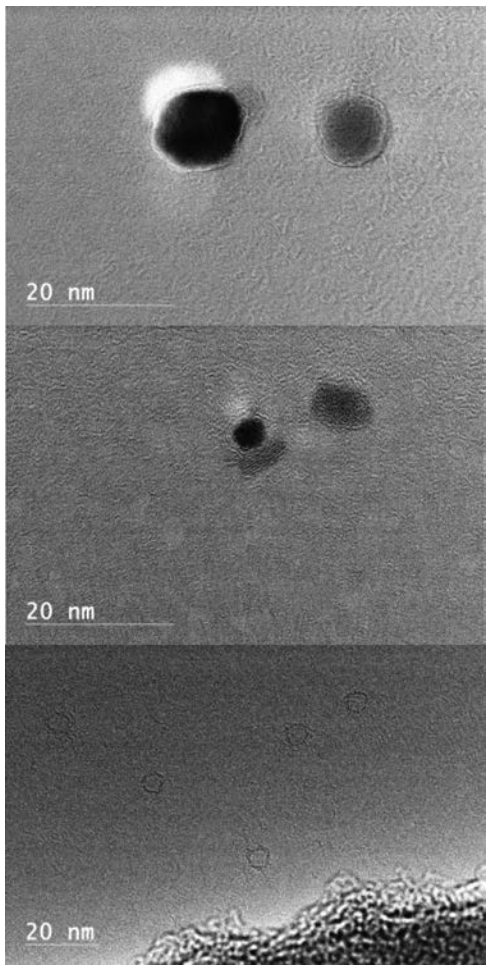

Figure 5. Transmission electron microscopy photos of HNO_3-purified graphene-encapsulated copper nanoparticles.

Thermogravimetric Analysis

The TGA analysis results are shown in Fig 6. There was a slight weight loss at 100 C for all samples, which was caused by the evaporation of H_2O. Then the curve was gradual for each sample until an abrupt weigh loss occurred at above 300 C.

The sample treated at 600 C, 30 min, 10 C/min, and 600 sccm started to have a sudden weight loss from 350 C, and ended at 430 C, indicating that this sample had the worst thermal stability. The

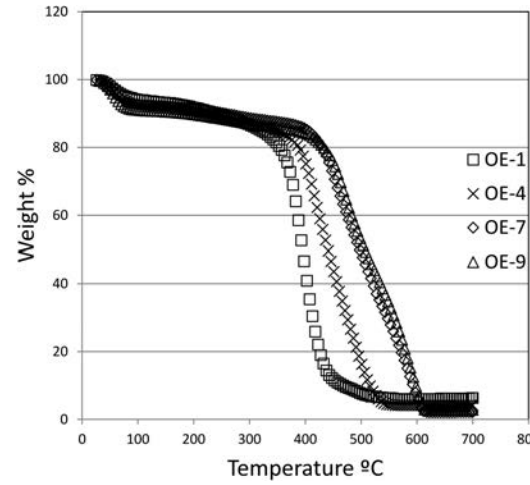

Figure 6. Thermogravimetric analysis graph for samples treated with parameter groups 1, 4, 7, and 9.

Table 4. Yield of graphene-encapsulated copper nanoparticles postheated at 200 C, 300 C, and 500 C.

Sample ID	Weight loss (%)
OE-7-200	3.99
OE-7-300	35.54
OE-7-500	91.43

sample treated at 800 C, 30 min, 15 C/min, and 1800 sccm resulted in better thermal stability, with an abrupt weight loss starting from 400 C, and ending at above 500 C. Sample treated at 1000 C, 30 min, 20 C/min, 1200 sccm and 1000 C, 90 min, 15 C/min, 600 sccm had similar weight loss curves, and these two groups presented the best thermal stability, which started to have a great weight loss from 450 C, while ended at above 600 C, and the slope was much flatter than the other two curves. Results also implied that temperature was more important than the other parameters.

The Effect of Postheat Treatment on the Crystallinity of Graphite

Table 4 shows the weight loss of GECNs postheated at 200 C, 300 C, and 500 C, respectively. GECNs were stable during postheat treatment at 200 C, with a weight loss of 4%. The weight loss was attributed to water vaporization, and no oxidation reaction occurred. When postheated at 300 C, the weight loss increased suddenly to 36%. Amorphous carbon was believed to combust and contributes mainly to the weight loss. Further increase in temperature up to 500 C resulted in 91% weight loss. At this point, all amorphous carbon might be gone or reconfigured. Copper nanoparticles might also be changed into other forms. Otherwise, the weight loss should not be over 90%. Further study needs to be continued.

The phase change of graphite and copper is illustrated in the XRD spectra (Fig 7). GECNs post heated at 200 C showed almost no changes in copper and graphite peaks; for that post heated at 300 C, the intensity of Cu_2O peak at around 37 was strengthened, and the intensity of Cu peak decreased. However, the improvement of graphite crystallinity could not be determined; further increase in temperature to 500 C resulted in almost complete oxidation of Cu atoms and the formation of Cu_2O and CuO. A sharp graphite

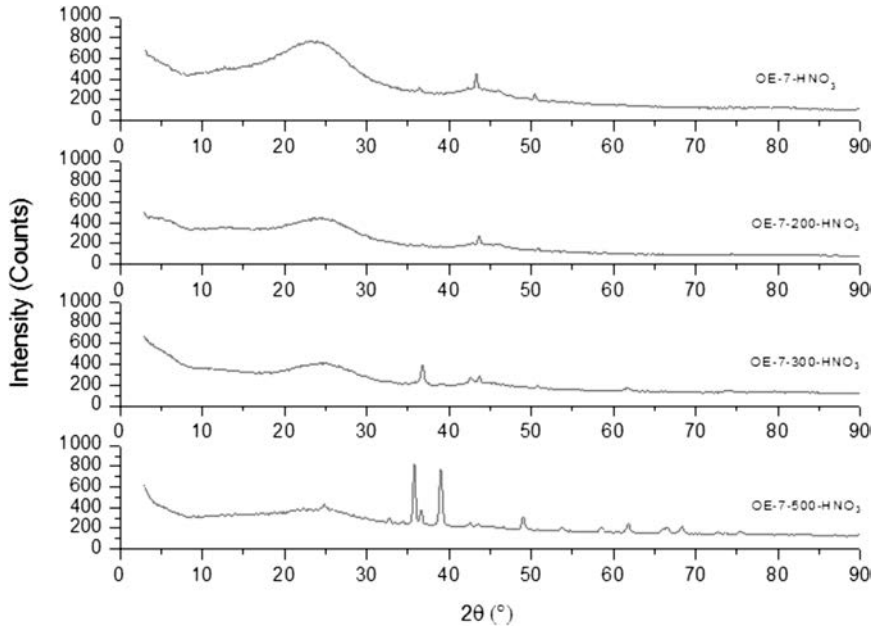

Figure 7. X-ray diffraction spectroscopy spectra of the graphene-encapsulated copper nanoparticles (GECNs) treated at 1000 C, 30 min, 20 C/min, and 1200-sccm gas flow rate, and the same GECNs postheated at 200 C, 300 C, and 500 C in air.

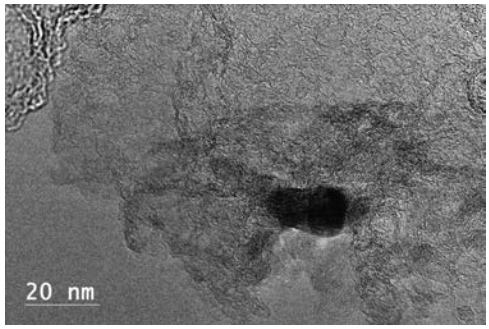

Figure 8. Transmission electron microscopy image of graphene-encapsulated copper nanoparticles postheated at 500 C in air.

peak appears at around $2\theta = 26$ for the GECNs postheated at 500 C, indicates that the crystallinity was improved after the postthermal treatment. The graphite peak was shifted to the right with the increase of postheat temperature, and finally close to $2\theta = 26$. Research has proved that graphene is stable in air, no changes occurred even under thermal treatment (Hsieh et al 2013). The improvement of graphite should be contributed by the decrease of amorphous carbon.

Figure 8 shows the morphology of sample postheated at 500 C. More graphene bands were obtained after the thermal oxidation. Part of the amorphous carbon was combusted, and part of them was transformed into graphene structures. Postheat treatment proved to be a feasible way to improve the crystallinity of the graphite.

CONCLUSIONS

The orthogonal experimental design was applied to characterize the synthesized lignin-based GECNs. Results revealed that temperature played the most important role in the growth of graphene. High temperature was preferred to obtain less defect sites. Complicated reactions existed during the annealing process. A feasible way to improve graphite crystallinity was postheat treatment. The data suggested the optimum synthesis parameters as 1000 C, 30 min duration time, 20 C/min temperature rising ramp, and 1200-sccm argon gas flow rate.

ACKNOWLEDGMENTS

The authors would like to acknowledge Domtar Corp., North Carolina for providing kraft lignin for this study. This manuscript was approved for publication as Journal Article No. SB 858 of the Forest and Wildlife Research Center, Mississippi State University.

REFERENCES

Athanassiou EK, Grass RN, Stark WJ (2006) Large-scale production of carbon-coated copper nanoparticles for sensor applications. Nanotechnology 17(6):1668-1673.

Chae SJ, Güneş F, Kim KK, Kim ES, Han GH, Kim SM, Shin H-J, Yoon S-M, Choi J-Y, Park MH, Yang CW, Pribat D, Lee YH (2009) Synthesis of large-area graphene layers on poly-nickel substrate by chemical vapor deposition: Wrinkle formation. Adv Mater 21(22):2328-2333.

Chen C-S, Hsieh C-K (2014) Effects of acetylene flow rate and processing temperature on graphene films grown by thermal chemical vapor deposition. Thin Solid Films 584:265-269.

Coates J (2000) Interpretation of infrared pectra, a practical approach. John Wiley & Sons Ltd, Chichester, England.

Gotoh K, Kinumoto T, Fujii E, Yamamoto A, Hashimoto H, Ohkubo T, Itadani A, Kuroda Y, Ishida H (2011) Exfoliated graphene sheets decorated with metal/metal oxide nanoparticles: Simple preparation from cation exchanged graphite oxide. Carbon 49(4):1118-1125.

Host JJ, Vinayak P, Teng, Mao-Hua (1998) Systematic study of graphite encapsulated nickel nanocrystal synthesis with formation mechanism implications. J Mater Res 13(9):2547-2555.

Hsieh Y-P, Wang Y-W, Ting C-C, Wang H-C, Chen K-Y, Yang C-C (2013) Effect of catalyst morphology on the quality of CVD grown graphene. J Nanomater 2013:1-6.

Huang C-H, Wang HP, Chang J-E, Eyring EM (2009) Synthesis of nanosize-controllable copper and its alloys in carbon shells. Chem Commun (Camb) 31:4663-4665.

Lee S, Hong J, Koo JH, Lee H, Lee S, Choi T, Jung H, Koo B, Park J, Kim H, Kim Y-W, Lee T (2013) Synthesis of few-layered graphene nanoballs with copper cores using solid carbon source. ACS Appl Mater Interfaces 5(7): 2432-2437.

Leng W, Barnes HM, Yan Q, Cai Z, Zhang J (2016) Low temperature synthesis of graphene-encapsulated copper nanoparticles from kraft lignin. Mater Lett 185:131-134.

Mun SP, Cai Z, Zhang J (2013) Fe-catalyzed thermal conversion of sodium lignosulfonate to graphene. Mater Lett 100:180-183.

Ou Q, Tanaka T, Mesko M, Ogino A, Nagatsu M (2008) Characteristics of graphene-layer encapsulated nanoparticles fabricated using laser ablation method. Diamond Related Materials 17(4-5):664-668.

Sun Z, Raji A-RO, Zhu Y, Xiang C, Yan Z, Kittrell C, Samuel E, Tour JM (2012) Large-area bernal-stacked bi-, tri-, and tetralayer graphene. ACS Nano 6(11):9790-9796.

Tarendash AS (2006) Let's review chemistry: The physical setting (4th ed.). Library of Congress Cataloging-in-Publication Datapp, New York, NY.

Wang K (2013) Laser based fabrication of graphene, advances in graphene science. Page 77-95 *in* M. Aliofkhazraei, ed. Advances in graphene science. Intech. http://www.intechopen.com/books/advances-in-graphene-science/laser-based-fabrication-of-graphene.

Wang S, Huang X, He Y, Huang H, Wu Y, Hou L, Liu X, Yang T, Zou J, Huang B (2012) Synthesis, growth mechanism and thermal stability of copper nanoparticles encapsulated by multi-layer graphene. Carbon 50(6): 2119-2125.

Wu WaZ, Zhu Z, Liu Z, Xie Y, Zhang, J, Hu T (2003) Preparation of carbon-encapsulated iron carbide nanoparticles by an explosion method. Carbon 41(2):317-321.

Yang H, Yan R, Chen H, Lee DH, Zheng C (2007) Characteristics of hemicellulose, cellulose and lignin pyrolysis. Fuel 86(12-13):1781-1788.

Zhou G, Taylor G, Polle A (2011) FTIR-ATR-based prediction and modelling of lignin and energy contents reveals independent intra-specific variation of these traits in bioenergy poplars. Plant Methods 7(1):9.

Zou Z, Dai B, Liu Z (2013) CVD process engineering for designed growth of graphene. Sci Sin Chim 43(1):1-17.